AGU PUBLICATIONS

Water Resources Research

RESEARCH ARTICLE
10.1002/2014WR016348

Mathematical equivalence between time-dependent single-rate and multirate mass transfer models

D. Fernàndez-Garcia[1] and X. Sanchez-Vila[1]

[1]Department of Geotechnical Engineering and Geosciences, GHS-Hydrogeology Group, Technical University of Catalonia, UPC-BarcelonaTech, Barcelona, Spain

Key Points:
- Multirate mass transfer reduces to an effective time-dependent single-rate model
- The effective mass transfer coefficient directly relates to the memory function
- Results explain the scale-dependence of mass transfer rates

Correspondence to:
D. Fernàndez-Garcia,
daniel.fernandez.g@upc.edu

Citation:
Fernàndez-Garcia, D., and X. Sanchez-Vila (2015), Mathematical equivalence between time-dependent single-rate and multirate mass transfer models, *Water Resour. Res.*, *51*, 3166–3180, doi:10.1002/2014WR016348.

Received 3 SEP 2014
Accepted 31 MAR 2015
Accepted article online 6 APR 2015
Published online 3 MAY 2015

Abstract The often observed tailing of tracer breakthrough curves is caused by a multitude of mass transfer processes taking place over multiple scales. Yet, in some cases, it is convenient to fit a transport model with a single-rate mass transfer coefficient that lumps all the non-Fickian observed behavior. Since mass transfer processes take place at all characteristic times, the single-rate mass transfer coefficient derived from measurements in the laboratory or in the field vary with time $\omega(t)$. The literature review and tracer experiments compiled by Haggerty et al. (2004) from a number of sites worldwide suggest that the characteristic mass transfer time, which is proportional to $\omega(t)^{-1}$, scales as a power law of the advective and experiment duration. This paper studies the mathematical equivalence between the multirate mass transfer model (MRMT) and a time-dependent single-rate mass transfer model (t-SRMT). In doing this, we provide new insights into the previously observed scale-dependence of mass transfer coefficients. The memory function, $g(t)$, which is the most salient feature of the MRMT model, determines the influence of the past values of concentrations on its present state. We found that the t-SRMT model can also be expressed by means of a memory function $\varphi(t,\tau)$. In this case, though the memory function is nonstationary, meaning that in general it cannot be written as $\varphi(t-\tau)$. Nevertheless, the full behavior of the concentrations using a single time-dependent rate $\omega(t)$ is approximately analogous to that of the MRMT model provided that the equality $\omega(t)=-d\ln g(t)/dt$ holds and the field capacity is properly chosen. This relationship suggests that when the memory function is a power law, $g(t)\sim t^{1-k}$, the equivalent mass transfer coefficient scales as $\omega(t)\sim t^{-1}$, nicely fitting without calibration the estimated mass transfer coefficients compiled by Haggerty et al. (2004).

1. Introduction

Solute transport in porous media is often characterized by a combination of mass transfer processes occurring on a multiplicity of space and time scales. The significance and diversity of these processes have been recognized already for a long time [e.g., *van Genuchten and Wierenga*, 1976; *Neretnieks*, 1980; *Rao et al.*, 1980, 1982] due to its important effect on solute transport observed in laboratory and field studies. The most significant outcome of this multiplicity of scales is the widely found result that the advection-dispersion equation (ADE) can seldom be used to model reported laboratory and field data [e.g., *Scheidegger*, 1959; *Hoehn et al.*, 1998; *Harvey and Gorelick*, 2000; *Levy and Berkowitz*, 2003; *Cortis and Berkowitz*, 2004; *Fernàndez-Garcia et al.*, 2005; *Gouze et al.*, 2008; *Castro-Alcalá et al.*, 2011; *Pedretti et al.*, 2013].

At the small scale, experimental findings show that, for example, the sorption/desorption mechanism is often limited by the diffusive transport within the fluid phase of the intraparticle pores of the sediment grains [e.g., *Ball and Roberts*, 1991; *Pignatello and Xing*, 1996; *Luthy et al.*, 1997; *Rügner et al.*, 1999], thus characterized by the spatially variable distribution of pore sizes and shapes. This situation is extended when looking at the intermediate scale. Various authors [e.g., *Guswa and Freyberg*, 2002; *Zinn and Harvey*, 2003; *Liu et al.*, 2004; *Willmann et al.*, 2008; *Fernàndez-Garcia et al.*, 2009] have demonstrated that solute transport through heterogeneous aquifers with connected high-conductivity pathways and/or lenses of low-conductivity material is often better upscaled using an advection-dispersion mass transfer model. It is now widely accepted that anomalous (as opposed to Fickian) transport is more the rule rather than the exception. Observed deviations include the scale-dependence of dispersivity as well as the directional and time-dependence of apparent porosity [e.g., *Dagan*, 1989; *Gelhar*, 1993; *Carrera*, 1993; *Sanchez-Vila and Carrera*, 1997; *Rubin*, 2003; *Tartakovsky and Neuman*, 2008, and references included therein]. But, arguably the most salient feature of non-Fickian transport is tailing [*Carrera*, 1993], defined as the asymmetric shape of

breakthrough curves (BTCs) in log-log plot, which cannot be reproduced by the homogeneous medium ADE. Field BTCs typically display a sharp rising limb but decay slowly at late time. Most importantly, the decay limb often displays a power law behavior [*Farrell and Reinhard*, 1994; *Hadermann and Heer*, 1996; *Werth et al*., 1997]. A proper description of this late time behavior is important not only for practical reasons, i.e., time for clean-up below a threshold [e.g., *de Barros et al*., 2013], but also because the apparent ubiquity of power-law decay suggests that it is linked to physical processes [*Haggerty et al*., 2000; *Shapiro*, 2001; *Meigs and Beauheim*, 2001; *Cortis and Berkowitz*, 2004].

The increasing interest in non-Fickian transport has produced a huge amount of literature, including different competing models of transport in porous media that could properly represent field observations [e.g., *Carrera et al*., 1998; *Benson et al*., 2000; *Berkowitz et al*., 2006]. Among them, the multirate mass transfer (MRMT) model [*Haggerty and Gorelick*, 1995] is frequently employed. In essence, this model considers that the medium can be represented by an overlapping mobile and immobile continua. The latter is characterized by a distribution of immobile zones that exchange solute mass with the mobile zone with exchange mass fluxes that are proportional to concentration gradients (variable in space and time). This model has been successfully applied to interpret anomalous transport [*Carrera et al*., 1998; *McKenna et al*., 2001; *Haggerty et al*., 2004; *Sanchez-Vila and Carrera*, 2004; *Willmann et al*., 2008; *Fernàndez-Garcia et al*., 2009] and can easily address reactive transport [*Donado et al*., 2009; *Willmann et al*., 2010; *Martinez-Landa et al*., 2012].

Unfortunately, mass transfer processes complicate solute transport simulations and, therefore, many of the studies performed up to now, consider only a simple first-order mass transfer model [e.g., *van Genuchten and Wierenga*, 1976; *Harvey and Gorelick*, 2000; *Riva et al*., 2008; *Guan et al*., 2008]. This is, from a mathematical and numerical point of view, a very convenient approach. Yet, it does not represent correctly the underlying physical process in many cases (presence of multiple mass transfer rates). A first-order mass transfer coefficient can be intuitively seen as an upscaled value, variable in time, that properly accounts for the total mass being transferred from the mobile to the suite of immobile zones at any given time. As a result, fitted mass transfer coefficients are scale-dependent. *Haggerty et al*. [2004] reviewed a large number (316) of field and laboratory tests and reinterpreted them by fitting a single-rate mass transfer coefficient (termed ω in the following); the outcome was that such apparent coefficients scaled with time or travel distance as $\omega \propto t^{-1}$.

In this paper, we aimed at analyzing the conditions for which a time-dependent single-rate mass transfer coefficient can effectively represent the behavior of a multirate mass transfer model. The objective is to provide an understanding of the coefficient as an upscaled parameter. For this purpose, the paper first presents the single-rate mass transfer model with a mass transfer coefficient that is variable in time (termed t-SRMT model). Then, the condition for the equivalence of this model with a general MRMT model with constant (in time) parameters is explored in terms of the equivalence of the corresponding memory functions. Examples for common MRMT models are then presented. Finally it is shown that the t-SRMT adjusts properly to the scaling in the ω parameter observed and proposed by *Haggerty et al*. [2004].

2. Mathematical Models

2.1. The Multirate Mass Transfer Model (MRMT)

The multirate model describes mass transfer between a mobile domain and any number of immobile domains. Mass transfer between the former and any one of the latter is characterized by a coefficient $\alpha[T^{-1}]$. The model is fully characterized by the porosity density function of the immobile zones, defined by $\phi_{im}(\alpha)[T]$. The advection-dispersion equation for the MRMT model can be written as [*Haggerty and Gorelick*, 1995],

$$R_m\phi_m\frac{\partial c_m}{\partial t}+\int_0^\infty R_{im}(\alpha)\phi_{im}(\alpha)\frac{\partial c_{im}(\alpha)}{\partial t}d\alpha=\nabla\cdot(\phi_m\mathbf{D}\nabla c_m)-\nabla\cdot(\mathbf{q}c_m), \tag{1}$$

where $c_m[M/L^3]$ is the aqueous concentration in the mobile domain, $c_{im}(\alpha)[M/L^3]$ is the aqueous concentration in the α-immobile domain, $\mathbf{D}[L^2/T]$ is the hydrodynamic dispersion tensor, $\mathbf{q}[L/T]$ is the groundwater flux, $R_m[-]$ and $R_{im}(\alpha)[-]$ are, respectively, the retardation factors in the mobile and the α-immobile domain, and $\phi_m[-]$ is the porosity of the mobile domain. The total immobile porosity $\phi_{im}^{tot}[-]$ represents

the ratio of total volume of stagnant water to the total volume of the system. It can be determined by the sum of all individual immobile porosities, $\phi_{im}(\alpha)[T]$,

$$\phi_{im}^{tot} = \int_0^\infty \phi_{im}(\alpha) d\alpha. \tag{2}$$

The mass transfer equations needed to close the system are given as

$$\frac{\partial c_{im}(\alpha)}{\partial t} = \alpha(c_m - c_{im}(\alpha)), \forall \alpha, \tag{3}$$

where α is a lumped mass transfer coefficient that includes the effects of diffusion, sorption, and other mass transfer processes. The solution to the coupled system of equations provided by (1) and (3) involves the definition of initial and boundary conditions. The former are particularly relevant for the analysis of the memory functions presented later on.

2.2. The Time-Dependent Single-Rate Mass Transfer Model (t-SRMT)

The time-dependent mass transfer model describes mass transfer between a mobile domain and only one immobile domain. Yet, the model accounts for the different mass transfer processes taking place over various scales by employing a (single) mass transfer coefficient that evolves with time $\omega(t)$. The driving equations for the t-SRMT model can be written as follows

$$\mathcal{R}_m \theta_m \frac{\partial c_m}{\partial t} + \mathcal{R}_{im} \theta_{im} \frac{\partial c_{im}}{\partial t} = \nabla \cdot (\theta_m \mathbf{D} \nabla c_m) - \nabla \cdot (\mathbf{q} c_m), \tag{4}$$

$$\frac{\partial c_{im}}{\partial t} = \omega(t)(c_m - c_{im}), \tag{5}$$

where $c_{im}[M/L^3]$ is the aqueous concentration in the immobile domain, and $\omega(t)[T^{-1}]$ is the time-dependent mass transfer coefficient. Here c_{im} provides some representative value characterizing the ensemble of immobile domains. Correspondingly, $\omega(t)$ can be seen as an effective transfer coefficient that at any time provides information about the total mass being transferred between the mobile and the ensemble of immobile domains. The use of different notation to represent retardation factors and porosities in (4) and (5) with respect to that used in (1) and (3) is utilized here for convenience, as later on several equivalences between parameters from the two formulations are sought.

The objective of this paper is to analyze the equivalence between the two models. Nevertheless, it is important to highlight some fundamental phenomenological differences between them. The MRMT model represents multiple mass transfer processes that occur simultaneously in a porous medium. This includes different spatially distributed regions formed among others by stagnant water, clay layers and pods, intraparticles pores and fractures. In this model, mass transfer in each region is characterized by a constant-in-time mass transfer rate, which typically represents steady state diffusion in a thin region. Instead, the t-SRMT model describes "free" diffusion in a thick region where mass transfer changes over time to describe nonstationary diffusion conditions. The fact that most diffusion problems will fall between these two categories suggests that the combination of these two models provides the most adequate conceptual model. To explore the implications of such differences is beyond the scope of the present paper but we expect that these differences may be important to reactive transport simulations.

3. Development of Memory Functions

3.1. The Memory Function for the MRMT Model

The memory functions associated with both models can be derived by direct integration of the corresponding mass transfer equations. Let us first focus on the MRMT model. By integrating (3), the following equation for the concentration of each individual immobile zone is obtained

$$c_{im}(\alpha) = \int_0^t \alpha c_m(\tau) e^{-\alpha(t-\tau)} d\tau + e^{-\alpha t} c_{im}^0(\alpha), \tag{6}$$

where $c_{im}^0(\alpha)$ is the initial immobile concentration corresponding to the α-immobile zone. The total concentration in the immobile zone is obtained by integration in α

$$R_{im}^{tot}\phi_{im}^{tot}c_{im}^{tot}=\int_0^\infty R_{im}(\alpha)\phi_{im}(\alpha)c_{im}(\alpha)d\alpha, \tag{7}$$

where

$$R_{im}^{tot}\phi_{im}^{tot}=\int_0^\infty R_{im}(\alpha)\phi_{im}(\alpha)d\alpha. \tag{8}$$

At this stage, it is convenient to define $p(\alpha)[T]$ as the probability density function of mass transfer rates

$$p(\alpha)=\frac{R_{im}(\alpha)\phi_{im}(\alpha)}{R_{im}^{tot}\phi_{im}^{tot}}, \tag{9}$$

so that the total averaged concentration is the expected value of the immobile concentrations

$$c_{im}^{tot}=\int_0^\infty p(\alpha)c_{im}(\alpha)d\alpha. \tag{10}$$

Substituting (6) into (10) we obtain

$$c_{im}^{tot}=\int_0^t g(t-\tau)c_m(\tau)d\tau+\int_0^\infty p(\alpha)e^{-\alpha t}c_{im}^0(\alpha)d\alpha, \tag{11}$$

where $g(t)$ is the memory function [*Carrera et al.*, 1998] defined as

$$g(t)=\int_0^\infty \alpha p(\alpha)e^{-\alpha t}d\alpha. \tag{12}$$

Thus, as time evolves, the memory function emphasizes the different past values of the concentrations with respect to time, thus rendering temporal memory to the traditional local-in-time ADE.

3.2. The Memory Function for the t-SRMT Model

In the case of the t-SRMT model, by integrating the mass transfer equation (5), the concentration in the immobile zone (recall there is only one) is obtained by using the method of variation of parameters to solve linear ODEs with variable parameters. The result can be written as

$$c_{im}=\int_0^t \omega(\tau)c_m(\tau)\exp\left\{-\int_\tau^t \omega(\tau')d\tau'\right\}d\tau+\exp\left\{-\int_0^t \omega(\tau)d\tau\right\}c_{im}^0, \tag{13}$$

which can be conveniently rewritten by defining an alternative expression for a memory function

$$\varphi(t,\tau)=\omega(\tau)\exp\left\{-\int_\tau^t \omega(\tau')d\tau'\right\}, \tag{14}$$

so that the final expression for the immobile concentration becomes

$$c_{im}=\int_0^t \varphi(t,\tau)c_m(\tau)d\tau+\exp\left\{-\int_0^t \omega(\tau)d\tau\right\}c_{im}^0. \tag{15}$$

Regardless of the initial condition in the immobile zone, we see that the memory function of the t-SRMT model is fundamentally different from that of the MRMT. The t-SRMT model inherits a nonstationary memory function (14) that evolves with time; i.e., for any given time, the influence of the past mobile concentration values is different. Instead, the memory function of the MRMT model only depends on the lag time between the present time and the past concentration time. In mathematical words, the first term in the right-hand side of (11) is a convolution integral, which is not the case in (15). As analyzed in Appendix A, the only particular case when these two integrals could be identical is the trivial case of constant ω, which is equivalent to assuming that $p(\alpha)$ is characterized by a Dirac-delta function $p(\alpha)=\delta(\alpha-\omega)$.

4. Late-Time Behavior of BTCs

In order to obtain the late-time behavior of breakthrough curves (BTCs) for both mass transfer models and examine their similarities we follow the procedure of *Haggerty et al.* [2000]. Assuming that the

concentrations are initially null in all domains, i.e., $c_m^0=0, c_{im}^0(\alpha)=0, \forall\alpha$, and considering an instantaneous injection of a mass m_0 taking place at $t=0$ only in the mobile domain (that is to say that, initially, solute mass preferentially enters into the porous medium through high permeability areas),

$$c_m=m_0\delta(t), \tag{16}$$

the solution of the corresponding system of coupled transport equations to this particular problem is equivalent to examining the late-time behavior of the BTCs when the controlling process is back diffusion, i.e., this portion of the solution is fully dominated by the mass transfer from the immobile zones to the mobile one. This is equivalent to saying that the elapsed time (since injection) is larger than the characteristic advective time, but smaller than the largest characteristic mass transfer time (corresponding to the smallest α values). This situation implies for example that the mobile concentration has been washed out, and the driving processes are advection and back-diffusion, while dispersion in the mobile zone is insignificant and can be neglected (see a lucid discussion in *Haggerty et al.* [2000] for the relevance of the different processes at these large times). Assuming that the parameters are spatially constant and considering that there are no sources and sinks, the governing equation for both models written in one dimension (along the streamline s) is,

$$-q_s\frac{\partial c_m}{\partial s}=R_{im}^{tot}\phi_{im}^{tot}\frac{\partial c_{im}^{tot}}{\partial t}, \tag{17}$$

$$-q_s\frac{\partial c_m}{\partial s}=\mathcal{R}_{im}\theta_{im}\frac{\partial c_{im}}{\partial t}, \tag{18}$$

and integrating

$$c_m(s=L,t)=-\int_0^L R_{im}^{tot}\frac{\phi_{im}^{tot}}{q_s}\frac{\partial c_{im}^{tot}}{\partial t}ds', \tag{19}$$

$$c_m(s=L,t)=-\int_0^L \mathcal{R}_{im}\frac{\theta_{im}}{q_s}\frac{\partial c_{im}}{\partial t}ds'. \tag{20}$$

Knowing that the advective times can be defined, respectively, as

$$\bar{t}_\alpha=\int_0^L\frac{R_m\phi_m}{q_s}ds', \tag{21}$$

$$\bar{t}_\omega=\int_0^L\frac{\mathcal{R}_m\theta_m}{q_s}ds', \tag{22}$$

and assuming that $\partial c_{im}/\partial t$ and $\partial c_{im}^{tot}/\partial t$ slightly vary in space, it is possible to write compact expressions for the concentrations in the mobile zone at late times for each of the mass transfer models

$$c_m(s=L,t)=-\bar{t}_\alpha\frac{\partial c_{im}^{tot}}{\partial t}f_\alpha, \tag{23}$$

$$c_m(s=L,t)=-\bar{t}_\omega\frac{\partial c_{im}}{\partial t}f_\omega, \tag{24}$$

where f_α and f_ω are the field capacity coefficients associated with the MRMT model and t-SRMT model, respectively,

$$f_\alpha=\frac{R_{im}^{tot}\phi_{im}^{tot}}{R_m\phi_m}, \tag{25}$$

$$f_\omega=\frac{\mathcal{R}_{im}\theta_{im}}{\mathcal{R}_m\theta_m}. \tag{26}$$

In both cases, the resulting expressions are directly equivalent to that presented in equation (7) in *Haggerty et al.* [2000].

In order to find a closed-form solution for the late-time behavior of concentrations, we require an approximate solution of the immobile concentration c_{im} defined, respectively, in (11) and (15), so that we can evaluate the time derivatives. Knowing that c_m dies out as time increases, the two integrals depend strongly on

the initial mobile concentrations. Based on this, approximate solution of the immobile concentrations for late times can be obtained by considering $c_m = m_0\delta(t)$. In such a case,

$$c_{im}^{tot} = g(t)m_0, \tag{27}$$

$$c_{im} = \varphi(t,0)m_0, \tag{28}$$

and the late-time solution of mobile concentrations can be approximated as

$$c_m(s=L,t) = -m_0\bar{t}_\alpha f_\alpha \frac{dg(t)}{dt}, \tag{29}$$

$$c_m(s=L,t) = -m_0\bar{t}_\omega f_\omega \frac{\partial\varphi(t,0)}{\partial t}. \tag{30}$$

5. Analogy Between Mass Transfer Models

5.1. The General Expression

Here, we explore the relationship between the memory function of the MRMT model and the equivalent mass transfer coefficient $\omega(t)$ associated with the t-SRMT model for late-time concentrations. In order for both models to have the same solution, the following condition needs to be fulfilled, which stems from equating (29) with (30),

$$\bar{t}_\alpha f_\alpha \frac{dg(t)}{dt} = \bar{t}_\omega f_\omega \frac{\partial\varphi(t,0)}{\partial t}. \tag{31}$$

This identity would hold if ω and g are related by the following expression,

$$\omega(t) = -\frac{d\ln g(t)}{dt}, \tag{32}$$

so that equation (32) can be rewritten as

$$\bar{t}_\alpha f_\alpha \frac{dg(t)}{dt} = \bar{t}_\omega f_\omega \frac{\omega(0)}{g(0)}\frac{dg(t)}{dt}. \tag{33}$$

Assuming that both models have the same mobile porosity ($\phi_m = \theta_m$) and retardation factor, so that $\bar{t}_\alpha = \bar{t}_\omega$, equation (33) requires the following specific relationship between the field capacities of both models to hold

$$f_\omega = \chi f_\alpha, \tag{34}$$

where χ is the scaling factor defined as

$$\chi = \frac{g(0)}{\omega(0)}. \tag{35}$$

An expression similar to (32) was obtained by [*Ginn*, 2009] for a fully desorption problem.

Different MRMT models can be found in the literature. Such models are defined in terms of the memory function or the corresponding probability density function of mass transfer rates $p(\alpha)$ defined in (9). Among them, we can distinguish continuous and discrete models depending on the nature of the random variable α. The general formulation provided by equations (32) and (35) are now particularized for two common MRMT models, i.e., the discrete multirate model and the continuous truncated power law model. In the next sections, expressions will still be written in dimensional form. However, some figures will be presented using the following dimensionless variables to improve understanding,

$$x' = \frac{x}{L} \tag{36}$$

$$Pe = \frac{Lq}{\phi_m D} \tag{37}$$

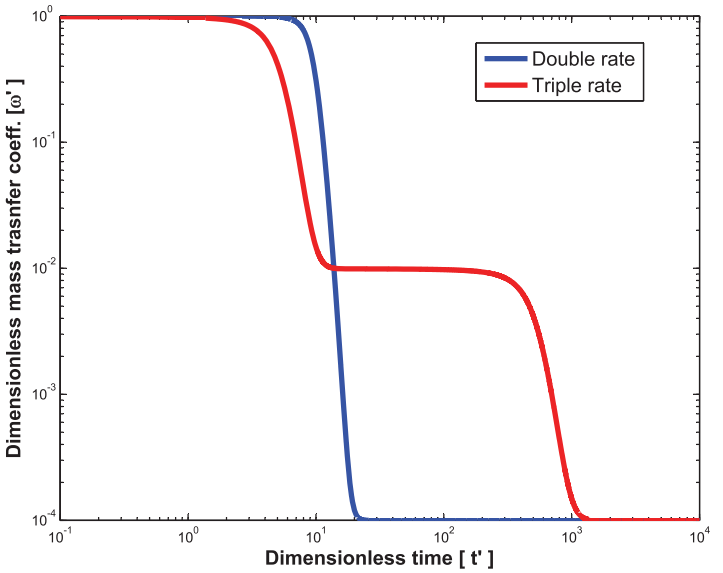

Figure 1. Time-dependence of the mass transfer coefficient needed to transform the t-SRMT model into the double MRMT model with parameters $P_1=P_2=1/2$, $\alpha'_1=0.0001$, $\alpha'_2=1$, and the triple MRMT model with parameters $P_1=P_2=P_3=1/3$, $\alpha'_1=0.0001$, $\alpha'_2=0.01$, and $\alpha'_3=1$.

$$t'=\frac{tq}{\phi_m R_m L} \tag{38}$$

$$\alpha'=\frac{\alpha L\phi_m R_m}{q} \tag{39}$$

$$\omega'=\frac{\omega L\theta_m \mathcal{R}_m}{q} \tag{40}$$

where t' is a dimensionless time equivalent to the number of pore volumes flushed in a soil column of length L, and Pe is the Peclet number.

5.2. The Discrete Multirate Model

Multiple rate models imply that the immobile sites can be characterized by many distinct rates, each one describing a different mass transfer process taking place simultaneously inside the porous media. This representation allows to include various mass transfer processes occurring over a wide range of scales (heterogeneity) and renders versatility to the model by simply choosing appropriate rate distributions. The probability density function of rate coefficients is written as

$$p(\alpha)=\sum_j P_j\delta(\alpha-\alpha_j), \tag{41}$$

where P_j is the probability of occurrence of the jth mass transfer rate so that

$$\sum_j P_j=1. \tag{42}$$

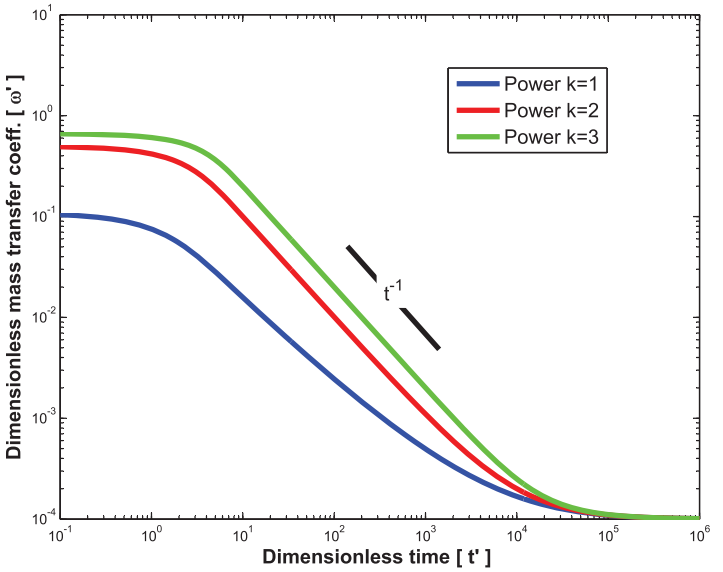

Figure 2. Time-dependence of the mass transfer coefficient needed to transform the t-SRMT model into the MRMT model for a truncated power law distribution of mass transfer rates with parameters $\alpha'_{min}=0.0001$ and $\alpha'_{max}=1$.

As a consequence, from (12) and (32), the memory function $g(t)$ and the corresponding $\omega(t)$ function are expressed as

$$g(t)=\sum_j P_j\alpha_j \exp(-\alpha_j t), \tag{43}$$

$$\omega(t)=\frac{\sum_j P_j\alpha_j^2\exp(-\alpha_j t)}{\sum_j P_j\alpha_j\exp(-\alpha_j t)}. \tag{44}$$

Typically, the late-time behavior in BTCs can be approximated by a small number of mass transfer coefficients [*Zhang et al.*, 2007]. In this context, the simple double rate model has been shown to capture a large portion of the BTCs in heterogeneous porous media [*Fernàndez-Garcia et al.*, 2009;

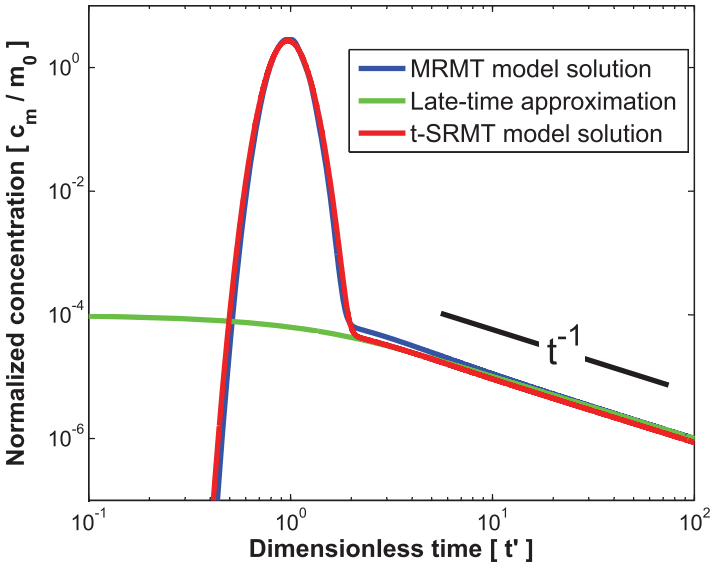

Figure 3. Comparison of the t-SRMT solution with the MRMT solution and the late-time approximation for a truncated power law distribution of mass transfer rates with parameters $x'=1$, $Pe=100$, $f_\alpha=1$, $k=1$, $\alpha'_{min}=0.0001$, $\alpha'_{max}=1$.

Li et al., 2011]. Figure 1 shows the time-dependence of the effective single-rate mass transfer coefficient needed to transform the t-SRMT model into the double and triple MRMT model. The double rate model is described by two distinct rate coefficients, α_1 and α_2, where $\alpha_2 \gg \alpha_1$, and we have that $\omega(t) \to \alpha_2$ for short times and $\omega(t) \to \alpha_1$ for very large times, with a monotonous transition in between. Similar behavior is observed for models with a larger number of mass transfer coefficients (an example of three rates is also provided in the figure).

In order to emulate the MRMT model with a time-dependent single-rate mass transfer coefficient, the scaling factor of the t-SRMT derived from (35) must be

$$\chi = \frac{\left(\sum_j P_j \alpha_j\right)^2}{\sum_j P_j \alpha_j^2}. \tag{45}$$

From the previous expression, it can be observed that the t-SRMT model will always inherit a smaller field capacity coefficient as compared to the corresponding MRMT model. If both models have the same field capacity coefficient with $\omega = -d\ln g/dt$, i.e., the resulting BTC of the t-SRMT and MRMT model will exhibit the same power law behavior but with different magnitude, or in other words, the t-SRMT will show larger concentration values. An obvious trivial case is the single-rate mass transfer model with the parameter constant in time. In such a case, from (44) and (45), it is found that $\omega = \alpha$ and $\chi = 1$ satisfy the conditions imposed for the equivalence of the two formulations.

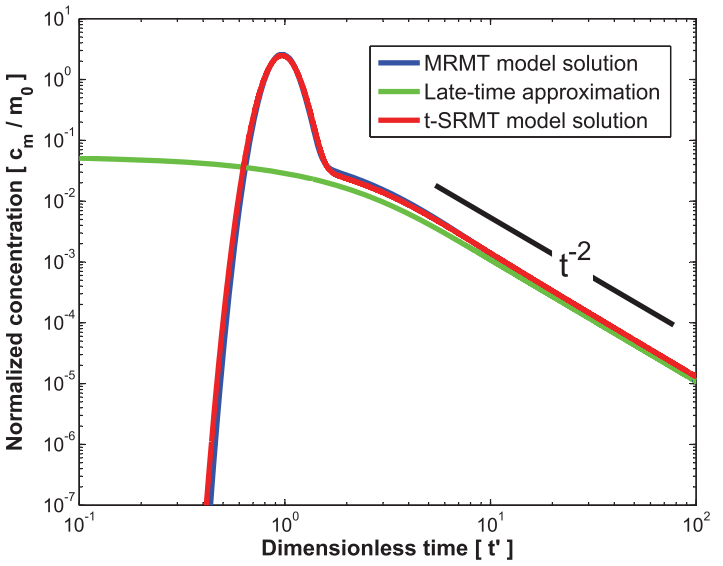

Figure 4. Comparison of the t-SRMT solution with the MRMT solution and the late-time approximation for a truncated power law distribution of mass transfer rates with parameters $x'=1$, $Pe=100$, $f_\alpha=1$, $k=2$, $\alpha'_{min}=0.0001$, $\alpha'_{max}=1$.

5.3. The Truncated Power Law Model

The often observed power law behavior in BTCs at late times has favored the use of the truncated power-law memory function in the interpretation of field, laboratory, and numerical observations [e.g., *Haggerty et al.*, 2000; *Fernàndez-Garcia et al.*, 2009; *Pedretti et al.*, 2013]. In this case, the probability density function of mass transfer rates is

Table 1. Multirate Series for Diffusion Models [After *Haggerty and Gorelick*, 1995]

	Multirate Series[a]	
Diffusion Geometry	α_j for $j=1,\ldots,N-1$	P_j for $j=1,\ldots,N-1$
Layered diffusion	$\frac{(2j-1)^2\pi^2}{4}\alpha$	$\frac{8}{(2j-1)^2\pi^2}$
Cylindrical diffusion[b]	$r_{0,j}^2\alpha$	$\frac{4}{r_{0,j}^2}$
Spherical diffusion	$j^2\pi^2\alpha$	$\frac{6}{j^2\pi^2}$

[a] $\alpha=D_a/a^2$ is the diffusion rate coefficient, where D_a is the apparent pore diffusion coefficient (ratio of the effective pore diffusion coefficient to the immobile zone retardation) and a is the distance from the center to the edge of the immobile zone.

[b] $r_{0,j}$ is the jth root of $J_0(x)$, where J_0 is the zero-order Bessel function of the first kind.

$$p(\alpha)=\mathcal{A}_1(k)I(\alpha)\alpha^{k-3}, k>0, \quad (46)$$

where $I(\alpha)$ is an indicator function that is equal to one when $\alpha_{min}\le\alpha\le\alpha_{max}$ and zero otherwise, and $\mathcal{A}_1(k)$ is a constant value that normalizes the probability density function to integrate to unity,

$$\mathcal{A}_1(k)=\begin{cases}(k-2)/(\alpha_{max}^{k-2}-\alpha_{min}^{k-2}) & \text{if } k\neq 2\\ 1/\ln(\alpha_{max}/\alpha_{min}) & \text{if } k=2\end{cases} \quad (47)$$

The corresponding memory function is given by

$$g(t)=\mathcal{A}_1(k)\int_{\alpha_{min}}^{\alpha_{max}}\alpha^{k-2}\exp(-\alpha t)d\alpha, \quad (48)$$

which can be written as

$$g(t)=\begin{cases}\mathcal{A}_1(k)\mathcal{A}_2(k-1,t)t^{1-k} & \text{if } t>0\\ \mathcal{A}_1(k)/\mathcal{A}_1(k+1) & \text{if } t=0\end{cases} \quad (49)$$

where

$$\mathcal{A}_2(k,t)=\Gamma(k,\alpha_{min}t)-\Gamma(k,\alpha_{max}t), \quad (50)$$

and $\Gamma(s,x)$ is the upper incomplete gamma function defined in integral form by $\Gamma(s,x)=\int_x^\infty t^{s-1}e^{-t}dt$.

The corresponding $\omega(t)$ function associated with the t-SRMT model, defined from (32), is better computed here as

$$\omega(t)=-\frac{1}{g(t)}\frac{dg(t)}{dt}, \quad (51)$$

The derivative of the memory function can written as

$$\frac{dg(t)}{dt}=-\mathcal{A}_1(k)\int_{\alpha_{min}}^{\alpha_{max}}\alpha^{k-1}\exp(-\alpha t)d\alpha, \quad (52)$$

or alternatively

$$\frac{dg(t)}{dt}=\begin{cases}-\mathcal{A}_1(k)\mathcal{A}_2(k,t)t^{-k} & \text{if } t>0\\ -\mathcal{A}_1(k)/\mathcal{A}_1(k+2) & \text{if } t=0\end{cases} \quad (53)$$

Substituting (49) and (53) into (51), we obtain

$$\omega(t)=\begin{cases}\mathcal{A}_2(k,t)/\mathcal{A}_2(k-1,t)t^{-1} & \text{if } t>0\\ \mathcal{A}_1(k+1)/\mathcal{A}_1(k+2) & \text{if } t=0\end{cases} \quad (54)$$

In the limit, when $t\to\infty$, we obtain that $\omega\to\alpha_{min}$. Also, when $\alpha_{max}t\ll 1$ and $\alpha_{min}t\approx 1$ the function $\mathcal{A}_2(k,t)$ becomes almost constant with time and equal to $\mathcal{A}_2(k,t)\approx\Gamma(k,1)-\Gamma(k,0)=e^{-1}$. Under these conditions, the memory function at late times is approximated as $g\sim t^{1-k}$, and the corresponding mobile concentration exhibits a power law behavior with an exponent equal to k, i.e., $c_m\sim t^{-k}$.

The final result is that ω decreases as $1/t$ for a range of times (the actual range depends on the k value). This effect is visualized in Figure 2, where ω is presented as a function of time for power law models with different k values. Furthermore, the scaling factor derived from (35) is a function of k given by

Table 2. Final Terms of Truncated Multirate Series [After *Haggerty and Gorelick*, 1995]

	Final Term in Multirate Series	
Diffusion Geometry	α_N	P_N
Layered diffusion	$\frac{3\alpha\left[1-\sum_{j=1}^{N-1}\frac{8}{(2j-1)^2\pi^2}\right]}{1-\sum_{j=1}^{N-1}\frac{96}{(2j-1)^4\pi^4}}$	$\left[1-\sum_{j=1}^{N-1}\frac{8}{(2j-1)^2\pi^2}\right]$
Cylindrical diffusion	$\frac{8\alpha\left[1-\sum_{j=1}^{N-1}\frac{4}{r_{0,j}^2}\right]}{1-\sum_{j=1}^{N-1}\frac{32}{r_{0,j}^4}}$	$\left[1-\sum_{j=1}^{N-1}\frac{4}{r_{0,j}^2}\right]$
Spherical diffusion	$\frac{15\alpha\left[1-\sum_{j=1}^{N-1}\frac{6}{j^2\pi^2}\right]}{1-\sum_{j=1}^{N-1}\frac{90}{j^4\pi^4}}$	$\left[1-\sum_{j=1}^{N-1}\frac{6}{j^2\pi^2}\right]$

$$\chi(k)=\frac{\mathcal{A}_1(k)\mathcal{A}_1(k+2)}{(\mathcal{A}_1(k+1))^2}. \tag{55}$$

We further compared the normalized BTC obtained with a MRMT model characterized by a power law memory function to the corresponding t-SRMT model solution given by (54) with the inclusion of the scaling factor χ provided by (55) for two particular cases of $k=1$ (Figure 3) and $k=2$ (Figure 4). Most importantly, these results demonstrate that despite the fact that the memory function of the t-SRMT model is nonstationary and the equivalence between the two models is, in principle, only valid at late times, the t-SRMT model can fully simulate the entire shape of the BTC for a wide range of k values with a very good approximation. Given that a Dirac-input is properly simulated with the t-SRMT model, the principle of superposition suggests that general input conditions can also be simulated with the same approach.

5.4. Other MRMT Models

One of the main advantages of the discrete MRMT is the possibility to simulate other diffusion models proposed in the literature (diffusion into spheres, cylinders, and limited layers), which are obtained as particular cases of the MRMT model by choosing appropriate values for α_j and P_j in (41) under certain conditions [*Haggerty and Gorelick*, 1995; *de Dreuzy et al.*, 2013]. For completeness, the series of these coefficients for

Table 3. Density Functions $p(\alpha)$ and Corresponding Memory Functions $g(t)$, Effective Time-Dependent Mass Transfer Coefficients $\omega(t)$, and Scaling Factors χ.

Model	$p(\alpha)$	$g(t)$	$\omega(t)$	χ
General	$p(\alpha)$	$\int_0^\infty \alpha p(\alpha)e^{-\alpha t}d\alpha$	$\frac{\int_0^\infty \alpha^2 p(\alpha)e^{-\alpha t}d\alpha}{\int_0^\infty \alpha p(\alpha)e^{-\alpha t}d\alpha}$	$\frac{\left(\int_0^\infty \alpha p(\alpha)d\alpha\right)^2}{\int_0^\infty \alpha^2 p(\alpha)d\alpha}$
Discrete multirate[a]	$\sum_j P_j\delta(\alpha-\alpha_j)$	$\sum_j P_j\alpha_j e^{-\alpha_j t}$	$\frac{\sum_j P_j\alpha_j^2 e^{-\alpha_j t}}{\sum_j P_j\alpha_j e^{-\alpha_j t}}$	$\frac{\left(\sum_j P_j\alpha_j\right)^2}{\sum_j P_j\alpha_j^2}$
Gamma	$\frac{1}{\gamma^\eta\Gamma(\eta)}\alpha^{\eta-1}e^{-\alpha/\gamma}$	$\gamma\eta(\gamma t+1)^{-\eta-1}$	$\frac{\eta+1}{t+\frac{1}{\gamma}}$	$\frac{\eta}{1+\eta}$
Power law[b]	$\mathcal{A}_1(k)I(\alpha)\alpha^{k-3}$	$\mathcal{A}_1(k)\mathcal{A}_2(k-1,t)t^{1-k}$	$\frac{\mathcal{A}_2(k,t)}{\mathcal{A}_2(k-1,t)}t^{-1}$	$\frac{\mathcal{A}_1(k)\mathcal{A}_1(k+2)}{(\mathcal{A}_1(k+1))^2}$
Lognormal[c]	$\frac{1}{\sqrt{2\pi}\sigma\alpha}e^{-\frac{(\ln(\alpha)-\mu)^2}{2\sigma^2}}$	$\sim -F'(t)$	$\sim\frac{F'(t)}{F'(t)}$	$\frac{e^{2\mu+\sigma^2}}{e^{2\mu+2\sigma^2}}$

[a]The discrete multirate model includes the limited diffusion models (cylindrical, layer, spherical) described in section 5.4. Parameters to be used to transform the discrete MRMT into diffusion models are given in Tables 1 and 2.

[b]Functions $\mathcal{A}_1$, $\mathcal{A}_2$, and I are defined in section 5.3. Expressions only valid for $k>0$ and $t>0$.

[c]The memory function of the lognormal distribution cannot be derived analytically. It is written here in terms of an approximate expression of the Laplace transform of the memory function, denoted as $F(t)$, given in section 5.4.

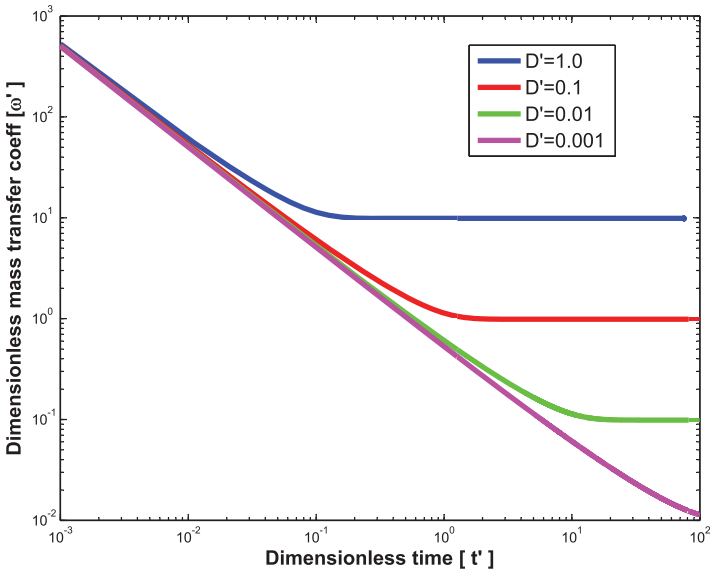

Figure 5. Time-dependence of the mass transfer coefficient needed to transform the t-SRMT model into the MRMT model for spherical diffusion.

the different geometries are shown in Tables 1 and 2. Modeling these processes usually requires a relatively large number ($N > 50$) of mass transfer rates. Also, a summary of widely used memory functions and corresponding $\omega(t)$ functions and scaling factors χ are listed in Table 3. As an example, we present the corresponding $\omega(t)$ function derived for a discrete model so as to reproduce spherical diffusion. Here, $D' = D_a L \phi_m R_m / a^2 q$, where D_a is the apparent pore diffusion coefficient (ratio of the effective pore diffusion coefficient to the immobile zone retardation), and a is the radius of the sphere. It is found that $\omega(t)$ decreases as $1/t$ for a range of times (see Figure 5), until the behavior brakes to become constant for large times ($t'D' \approx 0.1$). Both the time where behavior changes and the final asymptotic value depend on D'. Similar results are known in the literature of mass transfer. For instance, considering a purely diffusive problem (no advection), [*Rao et al.*, 1980] showed that the effective single-rate mass transfer coefficient determined to approximate diffusion into an individual sphere decreases with the experimental duration until the characteristic time approaches $a^2/15D_p$, where a is the radius of the sphere and D_p is the pore diffusivity.

Other continuous models such as the gamma and the lognormal distribution have also been employed in the literature [e.g., *Haggerty et al.*, 2000; *Lawrence et al.*, 2002]. Results are also listed in Table 3. All of them exhibit a $\omega(t)$ function that decreases with $1/t$ at late times. Here, we note that the memory function of the lognormal distribution cannot be derived analytically. Nevertheless, noticing that the memory function relates to the Laplace transform of the probability distribution of first-order mass transfer rates by

$$g(t) = -\frac{d}{dt}\mathcal{L}\{p(\alpha)\}(t) = -\frac{d}{dt}F(t), \tag{56}$$

a closed form approximation can be obtained via a modified version of the classic asymptotic Laplace's method [*Asmussen et al.*, 2013]. Based on this, the inverse Laplace transform of a lognormal distribution can be estimated as,

$$F(t) = \mathcal{L}\left\{p(\alpha)\right\}(t) = \frac{1}{\sqrt{1+W(te^{\mu}\sigma^2)}} \exp\left(-\frac{W^2(te^{\mu}\sigma^2)+2W(te^{\mu}\sigma^2)}{2\sigma^2}\right), \tag{57}$$

where $W(\cdot)$ is the Lambert W function which is defined as the solution of the equation $W(x)e^{W}(x) = x$.

Figure 6 provides the value of the scaling factor χ for the power law model and also for some of the models already presented before, as a function of the parameters defining the different models. We see that the t-SRMT model will always inherit a smaller field capacity coefficient relative to the corresponding MRMT model.

6. Comparison With Experimental Results

Haggerty et al. [2004] compiled a number of tracer experiments were mass transfer was the process controlling solute transport. They presented a review of reported experimental duration (t_{exp}) versus the fitted mass transfer coefficients from experiments performed in the field or in the laboratory (columns of different lengths).

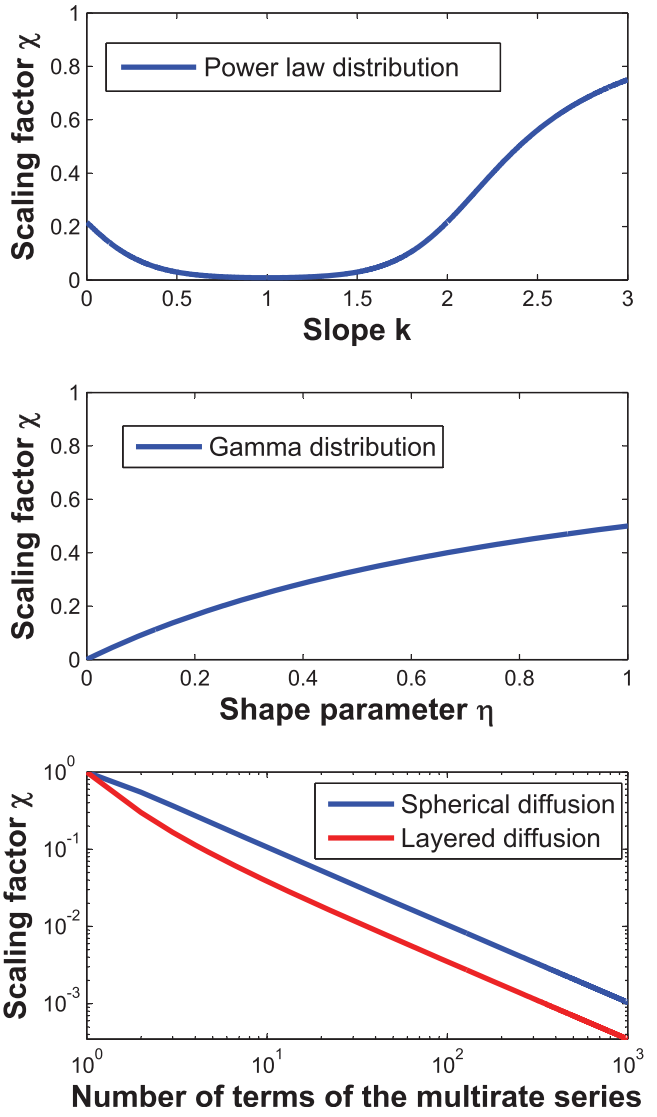

Figure 6. Scaling factor for different MRMT models: Truncated power law distribution of mass transfer rates, Gamma distribution of mass transfer rates, and diffusion models.

Remarkably, *Haggerty et al.* [2004] found a linear correlation between t_{exp} and the characteristic residence time in the immobile domain t_α. The corresponding correlation is given by $\log t_\alpha = 0.94 \log t_{exp} - 0.84$, with an $r^2 = 0.61$. The linear fit was performed with data coming from 271 experiments.

The aforementioned review included studies employing both single-rate mass transfer and diffusive mass transfer as a modeling method. Here, we focus only on those results obtained by curve-fitting the experimental BTCs with a constant single-rate mass transfer model, essentially described by

$$\frac{\partial c_{im}}{\partial t} = \bar{\omega}(c_m - c_{im}). \tag{58}$$

Contrary to the t-SRMT model, the parameter $\bar{\omega}$ does not evolve with time. It can be seen as an equivalent or apparent single-rate mass transfer coefficient. This parameter is somewhat related, but not equal, to our effective time-dependent mass transfer coefficient $\omega(t)$. By comparing the memory function associated to (58), written as $g(t) = \bar{\omega} \exp(-\bar{\omega} t)$, with the memory function of the t-SRMT model $\varphi(t, 0)$ given by evaluating (14) at $\tau = 0$, the following relationship between $\bar{\omega}$ and $\omega(t)$ can be determined,

$$\bar{\omega}(t_{exp}) = \frac{1}{t_{exp}} \int_0^{t_{exp}} \omega(\tau) d\tau. \tag{59}$$

Substituting (51) in (59), this expression is written in terms of the memory function by

$$\bar{\omega}(t_{exp}) = -\frac{1}{t_{exp}} \ln\left(\frac{g(t_{exp})}{g(0)}\right). \tag{60}$$

By noticing that $\bar{\omega}(t_{exp})$ is directly related to t_α^{-1}, we redrew the data reported by *Haggerty et al.* [2004] by plotting $\bar{\omega}$ versus t_{exp} in log −log space. From Figure 7, a linear relationship with a slope of −1 seems to properly fit the data. This behavior is very close to the one already presented for the generalized power law model. It could be written as a power law expression, finally resulting in $\bar{\omega} = 10 t_{exp}^{-1}$. In the same plot, the $\bar{\omega}$ values obtained using a power law model with $k = 1.5$, $k = 2$, and $k = 2.5$ (from equation (54)) is also displayed. A nice general fit is obtained without calibration. Notice that the t-SRMT solution is the same regardless of the k value adopted.

Recalling that most t-SRMT models (e.g., diffusion, power law, and gamma) predict a power-law behavior of first-order mass transfer rates with $\omega \sim t^{-1}$, it seems unlikely that one can distinguish the type of mass transfer model associated with the data set. From a different perspective, this can also be the reason why such a nice correlation was observed while including so many different experiments.

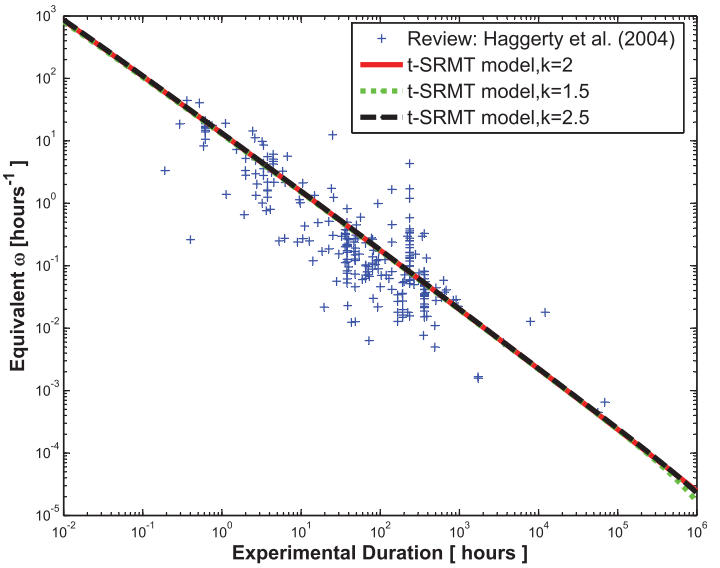

Figure 7. Comparison of the t-SRMT model assuming a power law model, from equation (60), with experimental data reviewed by *Haggerty et al.* [2004]. Notice that the t-SRMT solution is the same regardless of the *k* value adopted.

7. Conclusions

The MRMT model has been shown to correctly reproduce field observations of solute transport in porous media at different scales. Yet, in some cases a different model involving a single-rate mass transfer coefficient has been used for convenience. When this happens, the corresponding coefficient seems to display a temporal dependence.

We show the conditions under which the two models (MRMT and t-SMRT) can be considered mathematically equivalent. The MRMT model is fully characterized by a memory function which incorporates information from all previous times through a convolution integral in time, thus becoming stationary in time. The t-SRMT model is also fully characterized by a memory function, but in this case it is nonstationary. Despite this fundamental difference, the two models can be found approximately equivalent provided that the equality $\omega(t) = -d\ln g(t)/dt$ holds and the field capacity coefficient is properly chosen (by introducing an appropriate scaling factor χ). In such a case, the effective single-rate mass transfer coefficient is temporally variable and can be directly derived from the MRMT memory function.

This single-rate temporally variable coefficient displays a shape that is clearly related to the model chosen for the distribution of immobile sites. Most of the models analyzed lead to an upscaled ω decreasing linearly with time which agrees with the observations compiled by *Haggerty et al.* [2004] in a number of different sites worldwide.

Appendix A: On the Equivalence of Memory Functions

We analyze here the conditions under which the first integral in the right-hand side of (15) can be written as a convolution integral. A necessary condition of a function $f(t,\tau)$ to be written exclusively in terms of $(t-\tau)$ is that it verifies that

$$\frac{\partial f}{\partial t} = -\frac{\partial f}{\partial \tau}. \tag{A1}$$

Now we seek under which conditions equation (A1) holds, using function $\ln \varphi(t,\tau)$. It is found that

$$\frac{\partial \ln \varphi}{\partial t} = -\omega(t), \tag{A2}$$

$$-\frac{\partial \ln \varphi}{\partial \tau} = -\omega(\tau) - \frac{\partial}{\partial \tau}\ln \omega(\tau). \tag{A3}$$

The necessary condition for equation (A1) to hold is therefore that ω is a constant value.

Acknowledgments
Financial support from the Spanish Ministry of Education and Science (Project FEAR, Ref. CGL2012-38120), the European Union (project MARSOL, FP7-ENV-2013, Grant 619120), and the ICREA Academia Program are gratefully acknowledged.

References

Asmussen, S., J. L. Jensen, and L. Rojas-Nandayapa (2013), On the Laplace transform of the lognormal distribution, *Thiele Res. Rep.*, *6*(11), 1–23.

Ball, W. P., and P. V. Roberts (1991), Long-term sorption of halogenated organic chemicals by aquifer material. 2. Intraparticle diffusion, *Environ. Sci. Technol.*, *25*(7), 1237–1249.

Benson, D. A., S. W. Wheatcraft, and M. M. Meerschaerdt (2000), The fractional order governing equation of levy motion, *Water Resour. Res.*, *36*(6), 1413–1423.

Berkowitz, B., A. Cortis, M. Dentz, and H. Scher (2006), Modeling non-Fickian transport in geological formations as a continuous time random walk, *Rev. Geophys.*, *44*, RG2003, doi:10.1029/2005RG000178.
Carrera, J. (1993), An overview of uncertainties in modelling groundwater solute transport, *J. Contam. Hydrol.*, *13*(14), 23–48.
Carrera, J., X. Sánchez-Vila, I. Benet, A. Medina, G. Galarza, and J. Guimerà (1998), On matrix diffusion: Formulations, solution methods and qualitative effects, *Hydrogeol. J.*, *6*, 178–190.
Castro-Alcalá, E., D. Fernàndez-Garcia, J. Carrera, and D. Bolster (2011), Visualization of pore-scale mixing processes in a heterogeneous sand box aquifer, *Environ. Sci. Technol.*, *46*, 3228–3235, doi:10.1021/es201779.
Cortis, A., and B. Berkowitz (2004), Anomalous transport in classical soil and sand columns, *Soil Sci. Soc. Am. J.*, *68*(5), 1539–1548.
Dagan, G. (1989), *Flow and Transport in Porous Formations*, 461 pp., Springer, Berlin.
Dentz, M., and B. Berkowitz (2003), Transport behavior of a passive solute in continuous time random walks and multirate mass transfer, *Water Resour. Res.*, *39*(5), 1111, doi:10.1029/2001WR001163.
Donado, L., X. Sanchez-Vila, M. Dentz, J. Carrera, and D. Bolster (2009), Multicomponent reactive transport in multicontinuum media, *Water Resour. Res.*, *45*, W11402, doi:10.1029/2008WR006823.
de Barros, F. P. J., D. Fernàndez-Garcia, D. Bolster, and X. Sanchez-Vila (2013), A risk-based probabilistic framework to estimate the endpoint of remediation: Concentration rebound by rate-limited mass transfer, *Water Resour. Res.*, *49*, 1929–1942, doi:10.1002/wrcr.20171.
de Dreuzy, J.-R., A. Rapaport, T. Babey, and J. Harmand (2013), Influence of porosity structures on mixing-induced reactivity at chemical equilibrium in mobile/immobile Multi-Rate Mass Transfer (MRMT) and Multiple INteracting Continua (MINC) models, *Water Resour. Res.*, *49*, 8511–8530, doi:10.1002/2013WR013808.
Farrell, J., and M. Reinhard (1994), Desorption of halogenated organics from model solids, sediments, and soil under unsaturated conditions, 2, Kinetics, *Environ. Sci. Technol.*, *28*(1), 63–72.
Feehley, C. E., C. Zheng, and F. J. Molz (2000), A dual-domain mass transfer approach for modeling solute transport in heterogeneous aquifers: Application to the Macrodisperison Experiment (MADE) site, *Water Resour. Res.*, *36*(9), 2501–2515.
Fernàndez-Garcia, D., H. Rajaram, and T. H. Illangasekare (2005), Assessment of the predictive capabilities of stochastic theories in a three-dimensional laboratory test aquifer: Effective hydraulic conductivity and temporal moments of breakthrough curves, *Water Resour. Res.*, *41*, W04002, doi:10.1029/2004WR003523.
Fernàndez-Garcia, D., G. Llerar-Meza, and J. J. Gómez-Hernández (2009), Upscaling transport with mass transfer models: Mean behavior and propagation of uncertainty, *Water Resour. Res.*, *45*, W10411, doi:10.1029/2009WR007764.
Gelhar, L. W. (1993), *Stochastic Subsurface Hydrology*, 390 pp., Prentice Hall, Englewood Cliffs, N. J.
Ginn, T. R. (2009), Generalization of the multirate basis for time convolution to unequal forward and reverse rates and connection to reactions with memory, *Water Resour. Res.*, *45*, W12419, doi:10.1029/2009WR008320.
Gouze, P., T. Le Borgne, R. Leprovost, G. Lods, T. Poidras, and P. Pezard (2008), Non-Fickian dispersion in porous media: 1. Multiscale measurements using single-well injection withdrawal tracer tests, *Water Resour. Res.*, *44*, W06426, doi:10.1029/2007WR006278.
Guan, J., F. J. Molz, Q. Zhou, H. H. Liu, and C. Zheng (2008), Behavior of the mass transfer coefficient during the MADE-2 experiment: New insights, *Water Resour. Res.*, *44*, W02423, doi:10.1029/2007WR006120.
Guswa, A. J., and D. L. Freyberg (2002), On using the equivalent conductivity to characterize solute spreading in environments with low-permeability lenses, *Water Resour. Res.*, *38*(8), 1132, doi:10.1029/2001WR000528.
Hadermann J., and W. Heer (1996), The Grimsel (Switzerland) migration experiment: Integrating field experiments, laboratory investigations and modelling, *J. Contam. Hydrol.*, *21*, 87–100.
Haggerty, R., and S. M. Gorelick (1995), Multiple-rate mass transfer for modeling diffusion and surface reactions in media with pore-scale heterogeneity, *Water Resour. Res.*, *31*(10), 2383–2400.
Haggerty, R., S. A. McKenna, and L. C. Meigs (2000), On the late-time behaviour of tracer test breakthrough curves, *Water Resour. Res.*, *36*(12), 3467–3479.
Haggerty, R., C. F. Harvey, C. Freiherr von Schwerin, and L. C. Meigs (2004), What controls the apparent timescale of solute mass transfer in aquifers and soils?, A comparison of experimental results, *Water Resour. Res.*, *40*, W01510, doi:10.1029/2002WR001716.
Harvey, C., and S. M. Gorelick (2000), Rate-limited mass transfer or macrodispersion: Which dominates plume evolution at the Macrodispersion Experiment (MADE) site?, *Water Resour. Res.*, *36*(3), 637–650.
Hoehn, E., J. Eikenberg, T. Fierz, W. Drost, and E. Reichlmayr (1998), The Grimsel migration experiment: Field injection-withdrawal experiments in fractured rock with sorbing tracers, *J. Contam. Hydrol.*, *34*, 85–106.
Huang, H., and B. X. Hu (2000), Nonlocal nonreactive transport in heterogeneous porous media with interregional mass diffusion, *Water Resour. Res.*, *36*(7), 1665–1675.
Lawrence, A., X. Sanchez-Vila, and Y. Rubin (2002), Conditional moments of the breakthrough curves of kinetically sorbing solute in heterogeneous porous media using multirate mass transfer models for sorption and desorption, *Water Resour. Res.*, *38*(11), 1248, doi:10.1029/2001WR001006.
Levy, M., and B. Berkowitz (2003), Measurement and analysis of non-Fickian dispersion in heterogeneous porous media, *J. Contam. Hydrol.*, *64*(34), 203–226.
Li, Z., and M. L. Brusseau (2000), Nonideal transport of reactive solutes in heterogeneous porous media 6. Microscopic and macroscopic approaches for incorporating heterogeneous rate-limited mass transfer, *Water Resour. Res.*, *36*(10), 2853–2867.
Li, L., H. Zhou, and J. J. Gómez-Hernández (2011), Transport upscaling using multi-rate mass transfer in three-dimensional highly heterogeneous porous media, *Adv. Water Resour.*, *34*(4), 478–489.
Liu, G., C. Zheng, and S. M. Gorelick (2004), Limits of applicability of the advection-dispersion model in aquifers containing connected high-conductivity channels, *Water Resour. Res.*, *40*, W08308, doi:10.1029/2003WR002735.
Llopis-Albert, C., and J. E. Capilla (2009), Gradual conditioning of non-Gaussian transmissivity fields to flow and mass transport data: 3. Application to the Macrodispersion Experiment (MADE-2) site, on Columbus Air Force Base in Mississippi (USA), *J. Hydrol.*, *371*, 75–84.
Luthy, R. G., R. A. Aiken, M. L. Brusseau, S. D. Cunningham, P. M. Gschwend, J. J. Pignatello, M. Reinhard, S. J. Traina, W. J. Weber Jr., and J. C. Westall (1997), Sequestration of hydrophobic organic contaminants by geosorbents, *Environ. Sci. Technol.*, *31*(12), 3341–3347.
Martinez-Landaa, L., J. Carrera, M. Dentz, D. Fernàndez-Garcia, A. Nardi, M. Saaltink (2012), Mixing induced reactive transport in fractured crystalline rocks, *App. Geochem.*, *27*, 479–489, doi:10.1016/j.apgeochem.2011.09.016.
McKenna, S. A., L. C. Meigs, and R. Haggerty (2001), Tracer tests in a fractured dolomite 3. Double-porosity, multiple-rate mass transfer processes in convergent flow tracer tests, *Water Resour. Res.*, *37*(5), 1143–1154.
Meigs, L. C., and R. L. Beauheim (2001), Tracer tests in a fractured dolomite 1. Experimental design and observed tracer recoveries, *Water Resour. Res.*, *37*(5), 1113–1128.

Neretnieks, I. (1980), Diffusion in rock matrix: An important factor in radionuclide retardation?, *J. Geophys. Res.*, *85*(B8), 4379–4397.
Nkedi-Kizza, P., J. W. Biggar, H. M. Selim, T. van Genuchten, P. J. Wierenga, J. M. Davidson, and D. R. Nielsen (1984), On the equivalence of two conceptual models for describing ion exchange during transport through aggregated oxisol, *Water Resour. Res.*, *20*(8), 1123–1130.
Pedretti, D., D. Fernàndez-Garcia, D. Bolster, and X. Sanchez-Vila (2013), On the formation of breakthrough curves tailing during convergent flow tracer tests in three-dimensional heterogeneous aquifers, *Water Resour. Res.*, *49*, 4157–4173, doi:10.1002/wrcr.20330.
Pignatello, J. J., and B. Xing (1996), Mechanisms of slow sorption of organic chemicals to natural particles, *Environ. Sci. Technol.*, *30*(1), 1–11.
Rao, P. S. C., D. E. Rolston, R. E. Jessup, and J. M. Davidson (1980), Solute transport in aggregated porous media: Theoretical and experimental evaluation, *Soil Sci. Soc. Am. J.*, *44*(6), 1139–1146.
Rao, P. S. C., R. E. Jessup, and T. M. Addiscott (1982), Experimental and theoretical aspects of solute diffusion in spherical and nonspherical aggregates, *Soil Sci.*, *133*(6), 342–349.
Riva, M., A. Guadagnini, D. Fernàndez-Garcia, X. Sanchez-Vila, and T. Ptak (2008), Relative importance of geostatistical and transport models in describing heavily tailed breakthrough curves at the Lauswiesen site, *J. Contam. Hydrol.*,*101*, *1–13*.
Rubin, Y. (2003), *Applied Stochastic Hydrogeology*, 391 pp., Oxford Univ. Press, Oxford.
Rügner, H., S. Kleineidamm, and P. Grathwohl (1999), Long term sorption kinetics of phenanthrene in aquifer materials, *Environ. Sci. Technol.*, *33*(10), 1645–1651.
Sanchez-Vila, X., and J. Carrera (1997), Directional effects on convergent flow tracer tests, *Math. Geol.*, *29*(4), 551–569.
Sanchez-Vila, X., and J. Carrera (2004), On the striking similarity between the moments of breakthrough curves for a heterogeneous medium and a homogeneous medium with a matrix diffusion term, *J. Hydrol.*, *294*(1–3), 164–175, doi:10.1016/j.jhydrol.2003.12.046.
Scheidegger, A. E. (1959), An evaluation of the accuracy of the diffusivity equation for describing miscible displacement in porous media, in *Proceedings of the Theory of Fluid Flow in Porous Media Conference*, pp. 101–116, University of Oklahoma, Norman, Okla.
Shapiro, A. M. (2001), Effective matrix diffusion in kilometer-scale transport in fractured crystalline rock, *Water Resour. Res.*, *37*(3), 507–522.
Tartakovsky, A. M., and S. P. Neuman (2008), Effects of Peclet number on pore-scale mixing and channeling of a tracer and on directional advective porosity, *Geophys. Res. Lett.*, *35*, L21401, doi:10.1029/2008GL035895.
van Genuchten, M. Th., and P. J. Wierenga (1976), Mass transfer studies in sorbing porous media I. Analytical Solutions, *Soil Sci. Soc. Am. J.*, *40*(4), 473–480.
Wang, P. P., C. Zheng, and S. M. Gorelick (2005), A general approach to advective-dispersive transport with multirate mass transfer, *Adv. Water Resour.*, *28*, 33–42.
Werth, C. J., J. A. Cunningham, P. V. Roberts, and M. Reinhard (1997), Effects of grain-scale mass transfer on the transport of volatile organics through sediments, 2, Column results, *Water Resour. Res.*, *33*(12), 2727–2740.
Willmann, M., J. Carrera, and X. Sanchez-Vila (2008), Transport upscaling in heterogeneous aquifers: What physical parameters control memory functions?, *Water Resour. Res.*, *44*, W12437, doi:10.1029/2007WR006531.
Willmann, M., J. Carrera, X. Sanchez-Vila, O. Silva, and M. Dentz (2010), Coupling of mass transfer and reactive transport for non-linear reactions in heterogeneous media, *Water Resour. Res.*, *46*, W07512, doi:10.1029/2009WR007739.
Zhang, Y., Benson, D. A., and Baeumer, B. (2007), Predicting the tails of breakthrough curves in regional-scale alluvial systems, *Ground Water*, *45*(4), 473–484.
Zinn, B., and Ch. F. Harvey (2003), When good statistical models of aquifer heterogeneity go bad: A comparison of flow, dispersion, and mass transfer in connected and multivariate Gaussian hydraulic conductivity fields, *Water Resour. Res.*, *39*(3), 1051, doi:10.1029/2001WR001146.